JOURNAL OF MATERIALS SCIENCE 25 (1990) 2943–2948

Analytical electron microscopy of graphite-rich inclusions in sintered α-silicon carbide

W. BRAUE*, R. W. CARPENTER
Center for Solid State Science, Arizona State University, Tempe, Arizona 85287-1704, USA

Intragranular inclusions and multiphase regions at triple grain junctions in (B+C)-doped sintered α-SiC were investigated using analytical and high-resolution electron microscopy. Both regions were two-phase, composed of graphite and amorphous material. The triple junctions also contained pores. The amorphous regions were principally carbon and oxygen. Graphite was formed by partial transformation of the amorphous regions. Only the triple-junction regions contain typical impurities from the starting α-SiC powder, inferring that they are the main sinks for all grain-boundary/surface impurities in the material system.

1. Introduction

SiC-base structural ceramics made from either α- or β-type starting powders are well established in various fields of high-temperature application. Although different mechanisms of solid-state against liquid-phase sintering in the SiC system are still under discussion [1, 2], effective densification requires a suitable amount of a sintering aid like boron, while carbon is added to deoxidize the powder particle surfaces, remove free silicon by reaction, and retard grain growth. Various boron- and/or metal-impurity-bearing secondary phases have been characterized by small-probe microanalysis as grain-boundary precipitates or intragranular inclusions in both as-sintered and heat-treated SiC materials [3–5]. Graphite-rich particles are more frequently observed secondary phases in (B+C)-doped SiC. They either occur as irregular fibrous agglomerates in triple-grain junctions or as intragranular inclusions dispersed within the α-SiC matrix. In the material investigated here, graphite-rich inclusions are by far the dominant type of carbon phase, with porous triple-grain junctions observed occasionally. However, similar batches of (B+C)-doped α-SiC do not necessarily develop the same type of excess carbon particles. A recent comparison of commercial materials [6, 7] by auger electron spectroscopy showed that a large variety of different inclusions occurred including the simple pure graphite type, as well as boron carbides and non-stoichiometric boron-bearing particles. Obviously the final excess carbon-phase assemblages rely critically on the sources of raw materials and specific processing and sintering parameters.

Due to cavities and microcracks associated with them, excess carbon particles are regarded as failure-related under thermal cycling and creep-test conditions [8]. Graphite-rich inclusions in particular have been described qualitatively [4, 9, 10], but detailed analytical data and formation mechanisms have not been presented. This note summarizes both structural and microanalytical information for intragranular and triple-junction types of graphite inclusions in (B+C)-doped α-SiC. An interpretation relating the formation of the graphite inclusions to the chemical characteristics of the SiC powder and the polyphenylene precursor/deoxidant is given, and the overall microstructural development of the material is discussed.

2. Experimental procedures

The sample material was produced by sintering at 2000° C under 1 bar argon pressure, using a submicrometre-sized α-SiC sintering powder doped with 2 wt % boron and 2 wt % carbon. The carbon was added in a polyphenylene-H-resin during the mixing stage before compaction of the green body. This carbon precursor/deoxidant converts to amorphous carbon at about 800° C, with a yield of 85%. According to the supplier, this branched acetylene-terminated polyphenylene contained typically 10 to 15 p.p.m. sulphur and 1.5% oxygen as impurities in the uncured polymer [11]. The total metallic impurity concentration (principally aluminium, iron and calcium on the particle surfaces) of the starting SiC powder was less than 0.2 wt %.

TEM foils were prepared by conventional ion-beam thinning techniques. A Philips EM400 TEM/STEM fitted with a field-emission gun operating at 100 kV was used for microanalytical work. ELS spectra were collected with a serial Gatan spectrometer at 1 eV per channel, and with about equal beam convergence and acceptance half angles (10 mrad). A 10-nm TEM probe was typically adopted for both ELS and EDS work. In order to eliminate specimen contamination during small-probe experiments, microanalysis was performed using a low-drift cold stage with the specimen near liquid-nitrogen temperature. HREM images were taken in a JEOL 4000 EX at 400 kV.

* *Permanent address*: German Aerospace Research Establishment (DFVLR), Materials Research Institute, D-5000 Cologne 90, FRG.

0022–2461/90 $03.00 + .12 © *1990 Chapman and Hall Ltd.*

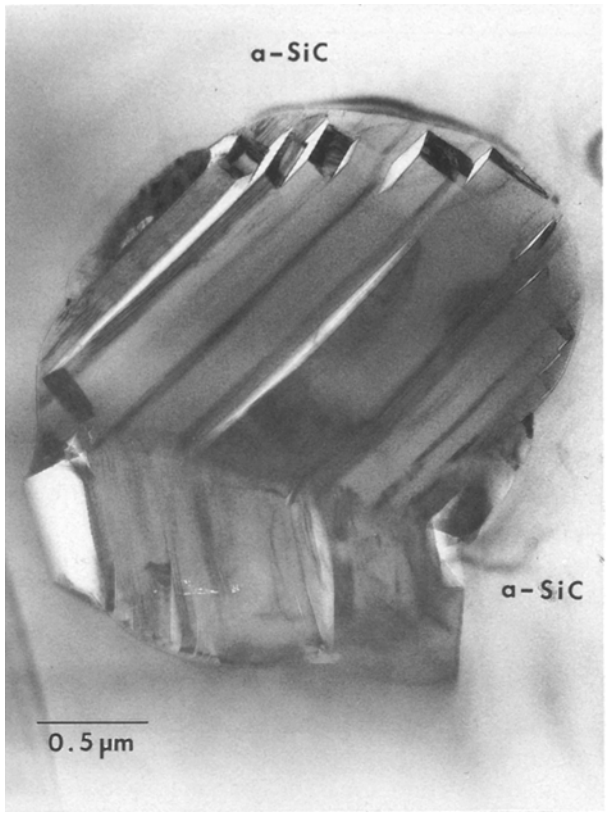

Figure 1 Typical twinned graphite-rich inclusion in an α-SiC matrix grain in (B+C)-doped α-SiC.

3. Results

The microstructure of the (B+C)-doped materials investigated consisted of α-SiC with 4H and 6H the most common polytypes. Typical grain size of the matrix was about 3 μm. Some grains displayed discontinuous grain growth, producing a bimodal grain-size distribution. The intragranular character of graphite-rich inclusions is a striking microstructural feature of this material. These inclusions exhibited an elliptical shape and consisted of thick graphite laths which are stacked parallel to a preferential orientation (Fig. 1). Twinning was commonly observed. Close to the circumference of the inclusions, the fibre bundles are often split by extended microcracking. Amorphous regions were observed between graphite fibre bundles in a number of these inclusions. The amorphous regions were observed at different tilts in diffraction contrast (and the contrast did not change), by HREM and by CBED. No evidence for microcrystals in the amorphous regions was observed. HREM imaging of a typical inclusion centre indicated that these areas actually consisted of amorphous carbon between adjacent graphite bundles (Fig. 2). Optical diffractograms taken from different positions within the graphite laths displayed varying degrees of structural disorder. The thickness of the amorphous regions between the graphite fibre bundles varied with position in the inclusion; that is, the graphite fibre bundles varied in width along their length. The occurrence of amorphous carbon was frequently restricted to the centre of an inclusion. A smooth boundary with no

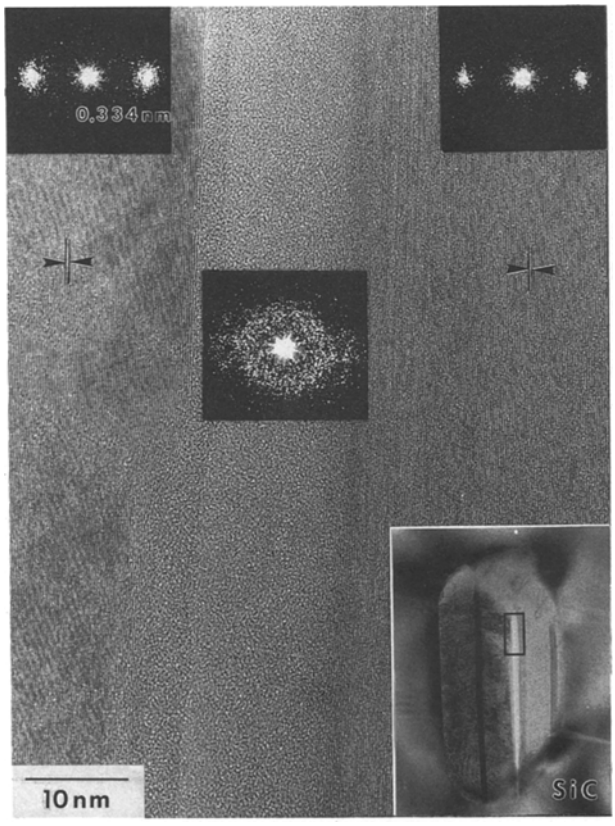

Figure 2 HREM image taken from an inclusion's centre. Inset, BF image of the corresponding inclusion. Note appropriate optical diffractograms characterizing both graphite and amorphous carbon regions.

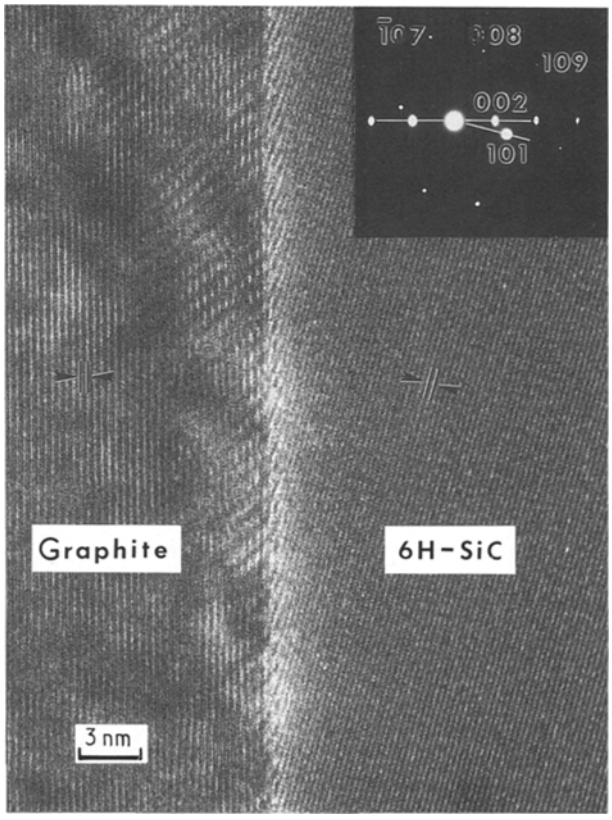

Figure 3 HREM image displaying the graphite/6H–SiC interface (same graphite inclusion as in Fig. 2). Fringes resolved correspond to $d_{(002)} = 0.334$ (graphite) and $d_{(101)} = 0.263$ nm (6H–SiC). See SAD pattern inserted (Orientation of 6H–SiC is close to [0 1 0]). Graphite {0 0 1} systematics are indicated by white line.

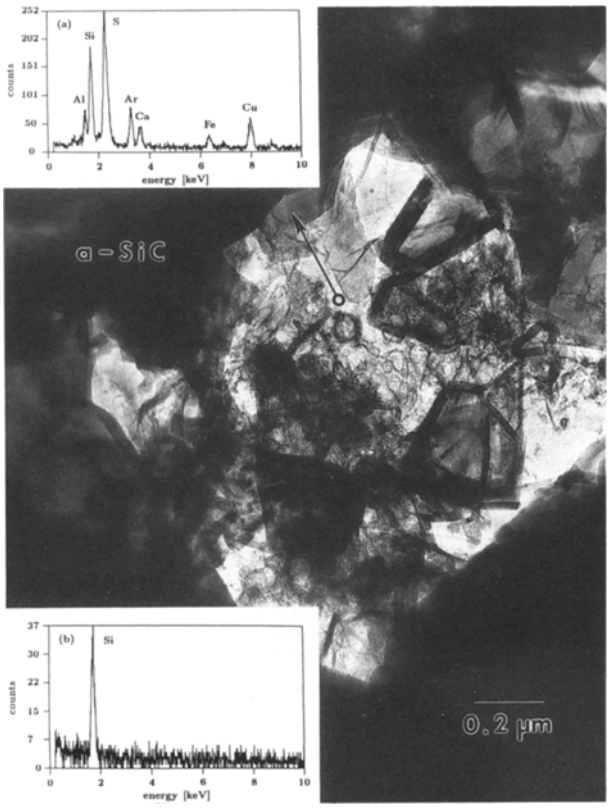

Figure 4 Porous triple-grain junction in (B+C)-doped α-SiC consisting of graphite microfilaments and interstitial areas of amorphous carbon. Circle marks position of upper EDS spectrum inset. Inset (a) spectrum for amorphous area in porous triple-grain junction; (b) hole count spectrum.

indication of interfacial reactions was established between the graphite inclusion and the 6H–SiC matrix phase (Fig. 3). This interface is obviously quite flat and well defined, as if a well-ordered epinucleation process for one crystal occurred on the surface of the other. Not enough of these interfaces were observed to determine whether a preferred low-energy orientation relationship existed, but in the general case one, or more than one, would be expected.

The microstructure of triple junctions had a quite different appearance, as shown in Fig 4. It consisted of turbostratic graphite fibres with thin interlayers of amorphous material between them. There were also pores in many triple junctions. These were evident in thick section images taken at 400 kV. In thin specimens the concentration of pores can easily be overestimated due to differential ion-thinning rates; not all triple junctions contained these multiphase regions. The volume number density of these triple junction regions was smaller than that of intragranular inclusions, and the inclusions were generally smaller in size. Figure 4 also shows an EDS spectrum taken from the amorphous region of the triple junction; the spectrum shows the amorphous region is an impurity sink, containing sulphur from the polyphenylene resin, silicon and metals from the SiC particle surfaces, and argon from the final thinning process. The accompanying hole spectrum shows that those peaks did not result from the microscope systems background. EDS spectra from amorphous regions in intragranular

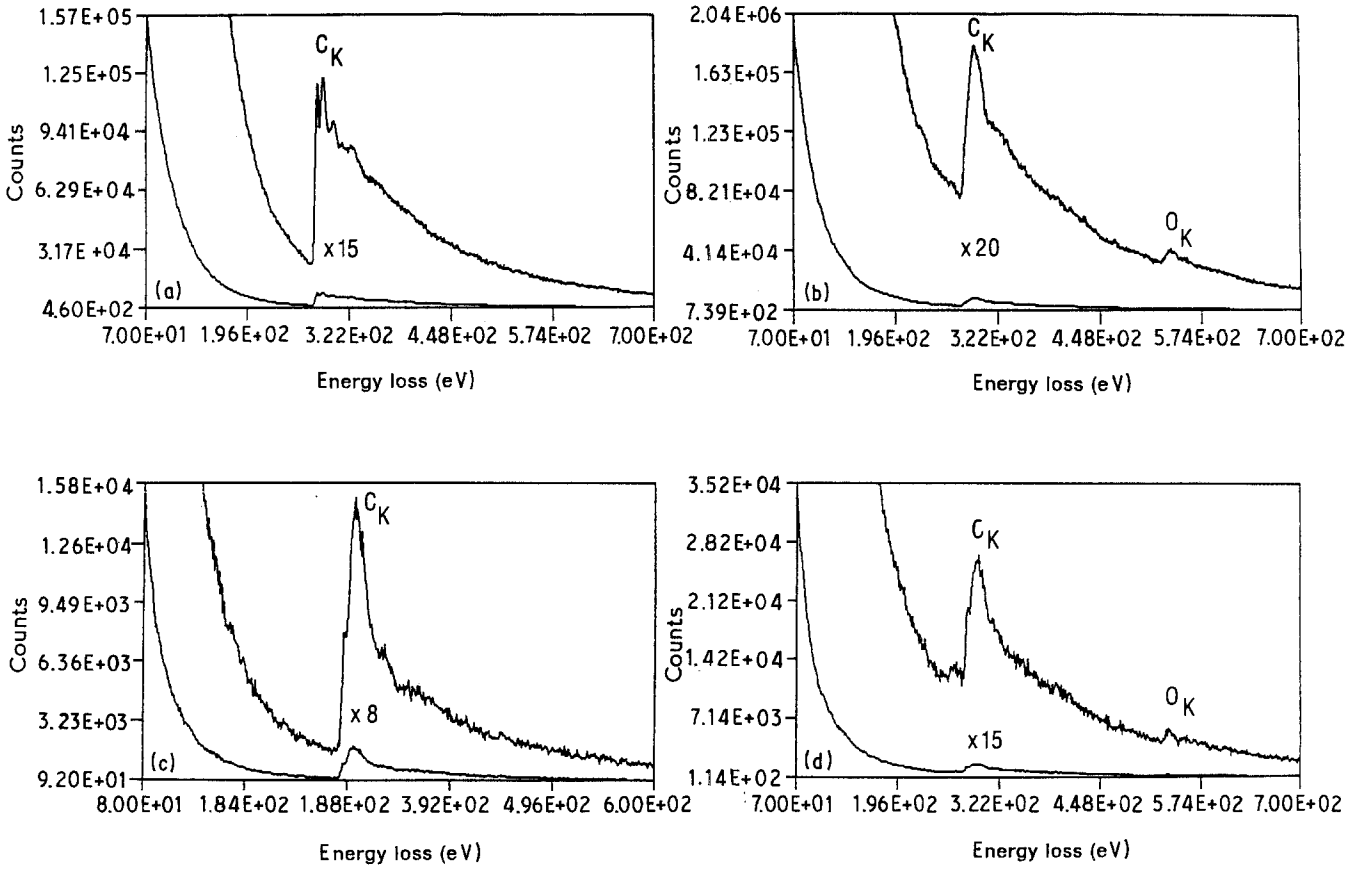

Figure 5 ELS spectra collected from different locations in both the graphite-rich inclusions and the porous triple-grain junctions in (B+C)-doped α-SiC. (a) Spectrum taken from graphite bundle in graphite-rich inclusion; (b) spectrum taken from amorphous carbon in graphite-rich inclusion (see Fig. 2); (c) spectrum corresponding to graphite-rich area within porous triple-grain junction (see Fig. 4); (d) spectrum taken from amorphous interstitial area in porous triple-grain junction (see Fig. 4).

inclusions did not indicate the presence of metallic impurities.

Significant differences in composition between the graphite fibres and amorphous regions were found using ELS microspectroscopy in both types of two-phase region. Results for the intragranular inclusions are given in Figs 5a and b; spectra from the graphite fibres exhibited only C–K edges, but spectra from amorphous regions exhibited a significant O–K edge in addition to a strong C–K edge. ELS spectra from graphite fibres and amorphous regions at triple grain junctions indicated the same distribution of oxygen, as shown in Figs 5c and d. No boron was detectable in ELS spectra from graphite or amorphous regions in either type of two-phase region. This result agrees with earlier research [4, 10]. We found no evidence for grain-boundary precipitates related to sintering aids, confirming the results of previous investigations [4, 12, 13].

The presence of oxygen in such a highly reducing environment at high temperature is unusual. The spectra were processed by a method described elsewhere to obtain oxygen and carbon concentrations [14]. Analysis of the spectrum of Fig. 5b showed the amorphous region contained 80 at % carbon and 20 at % oxygen, and also a trace of silicon. However the first plasmon to zero loss intensity ratio for this region was 0.59, indicating the specimen was rather thick and that this result should be considered semi-quantitative. Analysis of the triple junction spectrum of Fig. 5d yielded 68 at % carbon and 32 at % oxygen with no trace of silicon; for this specimen region the low loss intensity ratio was 0.25, indicating a much thinner specimen and quantitative results. These elemental analyses were performed by scaling the stripped edges to corresponding edges from SiC and SiO_2 standard specimens of known thickness, and also by comparing net integrated experimental peak intensity ratios to calculated theoretical ionization cross section ratios [15, 16]. All the results agree within $\pm 2\%$, thus the remarkably high oxygen concentration in the amorphous regions is correct.

These results confirm a similar earlier result for (B + C)-doped sintered SiC, from a different source, in which CBED and ELS were used to show that amorphous areas in two-phase graphite plus amorphous regions contained both carbon and oxygen. The microstructure in the earlier case was more complex, however, because the amorphous regions also contained SiC microcrystals, and had larger silicon and oxygen concentrations than in the present case [17].

The ELS spectra from oxygen-containing amorphous regions in the specimens of present interest also exhibited a small low-loss peak at 5 eV loss, and a similar small peak a few eV before the C–K edge onset. These small peaks were not present in spectra from the graphite fibres, and obviously are related to the presence of oxygen along with carbon in the amorphous regions, but the absorption mechanisms responsible are not yet explained.

The amorphous region of one intragranular inclusion exhibited triangular small particles with a high sulphur concentration (Fig. 6). Unfortunately these small particles were easily damaged by the electron beam, making quantification impossible. The morphology implied crystallinity, but tilting experiments failed to show the expected changes in diffraction contrast. We consider them crystalline but easily amorphized by the electron beam. These particles also contained a significant amount of copper, just as the amorphous region shown in Fig. 4 contained significant amounts of copper and iron. Hole count EDS spectra showed no trace of these elements in either case. These elements were either present in small amounts in one or both of these starting materials, or they were acquired by the specimen during some stage of processing. Evidently the processing itself caused concentration of these elements in the amorphous component of the two-phase regions, more so in the triple junctions than in the inclusions.

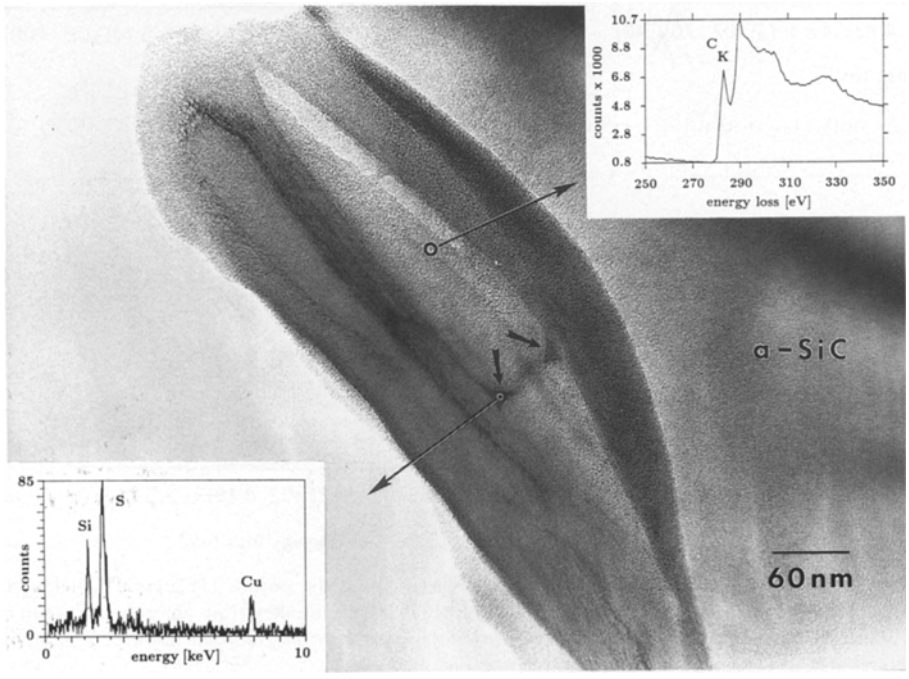

Figure 6 Graphite-rich inclusion displaying tiny triangular-shaped sulphur-rich grains located in the particle centre. Upper inset spectrum from graphite fibres. Lower inset spectrum from triangular grains.

4. Discussion

There are obvious microstructural similarities between the intragranular inclusions and the two-phase regions at triple-grain junctions, so the formation mechanism of both types of defects must be related, but they differ in detail. The surfaces of the SiC crystals bounding both types of two-phase regions were smooth, and exhibited no evidence of graphite formation interfaces moving into the bounding SiC grains from the two-phase regions. Most often the graphite fibre bundles were present at highest density adjacent to the bounding SiC crystals, and the amorphous carbon/oxygen regions were most numerous near the centre of the two-phase regions. During the first stage of processing the polyphenylene resin was distributed over the surfaces of the SiC particles. The resin converted to amorphous carbon at about 800° C, early in the sintering cycle, and absorbed oxygen from the SiC particle surfaces and the resin itself. Graphite nucleated at the interfaces of the bounding SiC grains with the amorphous carbon, and the transformation interfaces migrated towards the centres of the two-phase regions, but the graphitization reaction was incomplete, and did not consume all the amorphous carbon. The pores between the grains in the green body must have become a closed internal pore structure early in the sintering cycle, otherwise the oxygen observed in the amorphous carbon regions would not have been retained; it would have migrated out of the body as CO and/or SiO gas.

The different morphology of the graphite-fibre bundles in inclusions and triple junctions is probably directly related to the striking effect of boron on α-SiC grain growth and the nucleation of graphite at the α-SiC/amorphous carbon interfaces. According to earlier sintering experiments, boron additions exceeding 0.5 wt % in the batch result in rapid grain growth of the α-SiC [18]. This effect is responsible for the large average grain-size bimodal distribution we observed in the present materials, relative to the initial particle-size distribution. Prochazka [1] has shown that during this grain growth, immobile grain boundary inclusions can become intragranular inclusions when rapidly migrating boundaries move away from their original positions. Because the graphite fibre bundles appear to be nucleated at the interfaces between bounding α-SiC crystals and amorphous carbon, and the graphite fibres have a common orientation in inclusions (see Figs 1 and 2) but not in the triple-junction regions (see Fig. 4), it is highly probable that the amorphous carbon to graphite transformation began after appreciable grain boundary migration formed the intragranular inclusions. The graphite in inclusions was nucleated at different positions along a curved interface within a single SiC grain. On the other hand, graphite fibres in the triple-junction regions were nucleated at SiC/amorphous-carbon interfaces on three different surrounding grains, each with a different crystallographic orientation, and the fibres then grew toward the centre of the two-phase regions. This would be expected to result in a highly disordered array of graphite fibre bundles in triple-junction regions, which is what was observed. The misfit between graphite and 6H-SiC is rather large and favourable orientations for graphite nucleation on 6H–SiC probably also depend on the interface plane. The orientation relation shown in Fig. 3 is obviously one for which graphite nucleation can occur; here the graphite basal planes are about 20° away from {1 0 1} 6H planes. We occasionally observed [0 1 0] 6H approximately parallel to [0 1 0] graphite at these interfaces. A more detailed study of these orientation relationships is needed.

The rate of carbon transformation to graphite is affected by impurities in amorphous carbon. Certain metallic elements, such as iron, appear to reduce the onset of the transformation from above 2000 to near 1500° C. Marchand [19] has reported that in addition to the catalytic effects of certain dopants, graphitization kinetics may increase when sulphur and boron are present. These elements evidently stay in the amorphous carbon, so that in a closed system the impurity content of the amorphous carbon will increase as the fraction transformed to graphite increases. The effect of these impurities on the materials discussed here is to enhance the transformation rate of amorphous carbon to graphite at lower than normal temperatures. If an α-SiC compact not containing the impurities we observed were given the same processing cycle, we would expect to observe a somewhat different microstructure. In particular, much less grain growth would be expected, so the inclusion concentration within the α-SiC grains should be reduced or eliminated, and replaced by grain-boundary two-phase regions. Further, the transformation of amorphous carbon would be retarded, and the two-phase regions would contain more amorphous carbon than graphite.

The fact that impurities, particularly metallic impurities, are more highly concentrated in the amorphous regions associated with triple junctions than in similar regions of inclusions is clearly related to the continuous connection between grain boundaries and triple junctions. Most of these impurities entered the compact on the surface of α-SiC particles, and all of them have relatively low solubilities in SiC. Once boundaries migrate to form inclusions, fast transport paths to the inclusions are reduced or eliminated, but boundary diffusion or vapour transport by gaseous suboxides into the amorphous carbon regions at triple junctions is possible throughout the processing cycle. Thus the amorphous carbon at triple junctions becomes the only readily available internal impurity sink during most of the processing cycle.

It is interesting to note that two-phase regions containing graphite, amorphous carbon, oxygen and various other impurities occur in many other ceramic SiC-bearing materials synthesized by similar methods, but not necessarily containing the same starting compounds. We recently observed these regions in compacts of SiC with Al_2O_3 and Al_4C_3 sintered to form solutions of Al_2OC in SiC [20], in Al_2O_3 matrix composites reinforced with SiC whiskers [21], and in hot isostatically pressed SiC (HIP–SiC) [22]. In the latter case only an organic carbon precursor was added to the batch for the green body to retard exaggerated

grain growth during hot isostatic pressing; in this case the graphite regions were intergranular. No pores were observed because of the high hydrostatic pressure during densification.

5. Conclusions

Results from analytical (ELS and EDS) and high-resolution electron microscopy indicate similar formation mechanisms for graphite plus amorphous carbon/oxygen two-phase regions, in intragranular inclusions and porous triple grain junction regions in sintered (B+C)-doped α-SiC.

The amorphous carbon/oxygen in two-phase regions results from carbonization at about 800° C of a resin added earlier in processing. The graphite was formed by transformation of most of the amorphous carbon in each two-phase region later in the sintering cycle. The microstructure indicated that graphite nucleated at α-SiC/amorphous carbon interfaces. When a two-phase region was bounded by a single α-SiC crystal the resulting graphite had essentially one orientation, although high defect densities and twins were often present. When two-phase regions were bounded by more than one α-SiC crystal graphite fibre bundles of several orientations were formed. Intragranular two-phase regions were formed from grain boundary resin regions by motion of α-SiC grain boundaries during grain growth.

The impurities in the material (metals and oxygen from SiC particle surfaces and sulphur and oxygen from the resin) were concentrated in the amorphous portions of two-phase regions, with concentrations generally higher in polyphase triple junctions than in inclusions. The triple junction regions contained higher impurity concentrations because they were connected to the impurity sources, i.e. grain boundaries formed by intersection of α-SiC particle surfaces, throughout the whole sintering cycle. The grain boundaries and/or pore structure should be fast transport paths for impurities, by surface diffusion and/or vapour transport by CO and/or SiO gas and gaseous metal suboxides or other volatile compounds. The intragranular inclusions, once formed, were no longer connected to impurity sources by fast transport paths.

Acknowledgements

The sample material was provided by H. Hausner and H. Landferman, Technical University Berlin, FRG, who contributed important information on processing and sintering of (B+C)-doped α-SiC. Compositional details of the polyphenylene-H-resin are due to J. Fletcher from Hercules Inc., Wilmington, Delaware, USA. The assistance of D. J. Smith, CSSS, Arizona State University, in recording the HREM images is gratefully acknowledged. This study was conducted while W. Braue was with the CSSS, ASU. This research was supported by the Deutsche Forschungsgemeinschaft (DFG), FRG, the Center for Solid State Science, and the US Department of Energy (DE-FG02-87ER-45305).

References

1. S. PROCHAZKA in "Ceramics for High Performance Applications", edited by K. N. Katz (Brooke Hill, Chestnut Hill, Massachusettes, 1974) p. 239.
2. F. F. LANGE and T. K. GUPTA, *J. Amer. Ceram. Soc.* **59** (1976) 537.
3. M. RUEHLE and G. PETZOW, in "Surfaces and Interfaces in Ceramic and Ceramic–Metal Systems", edited by J. Pask and A. Evans (Plenum, New York, 1981) p.167.
4. A. J. BOURDILLON *et al.*, *J. Microsc.* **124** (1981) 49.
5. R. F. DAVIS *et al.*, *Scan. Elect. Micr.* **3** (1984) 1161.
6. R. HAMMINGER, G. GRATHWOHL and F. THUEMMLER, *Int. J. High Tech. Ceram.* **3** (1987) 129.
7. R. HAMMINGER, in Proceedings of the 3rd International Symposium on Ceramic Materials for Components and Engines, Las Vegas, Nevada, USA, November 27–30, 1988 (American Ceramic Society, Las Vegas, 1988) pp 115–126.
8. N. J. TIGHE, K. A. HARDMAN-RHYNE and Y. N. LU, in Proceedings of the 9th Annual Conference on Composites and Advanced Materials (1985) p. 835.
9. M. LANCIN *et al.*, *J. Mater. Sci.* **22** (1987) 1150.
10. H. YANG, T. E. MITCHELL and R. A. YOUNGMAN, in Proceedings of the 44th Annual Meeting of the Electron Microscopy Society of America, Albuquerque, New Mexico, USA, August 10–15, 1986, edited by G. Bailey (San Fransisco Press, San Fransisco, 1986) p. 474.
11. J. FLETCHER, Hercules Inc., private communication (1987).
12. K. L. MORE *et al.*, *J. Amer. Ceram. Soc.* **69** (1986) 695.
13. W. D. CARTER *et al.*, *Adv. Ceram. Mater.* **3** (1986) 62.
14. W. M. SKIFF, H. L. TSAI and R. W. CARPENTER, *Mater. Res. Soc. Symp. Proc.* **59** (1987) 241.
15. R. F. EGERTON, *Ultramicrosc.* **4** (1979) 169.
16. W. M. SKIFF *et al.*, *ibid.* **25** (1988) 47.
17. W. M. SKIFF and R. W. CARPENTER, in Proceedings of the 40th Annual Meeting of the Electron Microscopy Society of America, Washington, D.C., USA, August 9–13, 1982, edited by G. Bailey (San Fransisco Press, San Fransisco 1982) p. 564.
18. W. BOECKER and H. HAUSNER, *Powder Met. Int.* **10** (1978) 87.
19. A. MARCHAND, *Chem. Phys. Carbon* **7** (1971) 155.
20. R. W. CARPENTER, W. BRAUE and R. A. CUTLER, in Proceedings of the 45th Annual Meeting of the Electron Microscopy Society of America, Baltimore, Maryland, USA, August 2–7, 1987, edited by G. Bailey (San Fransisco Press, San Fransisco 1987) p. 306.
21. W. BRAUE, R. W. CARPENTER and D. J. SMITH, in Proceedings of the 46th Annual Meeting of the Electron Microscopy Society of America, Milwaukee, Wisconsin, USA, August 7–12, 1988, edited by G. Bailey (San Fransisco Press, San Fransisco 1988) p. 734.
22. W. BRAUE, J. GOERING and G. ZIEGLER, in Proceedings of the 3rd International Symposium on Ceramic Materials for Components and Engines, Las Vegas, Nevada, USA, November 27–30, 1988 (American Ceramic Society, 1989) pp. 817–830.

Received 15 February
and accepted 20 June 1989